International Journal of Nanomedicine

Dovepress
open access to scientific and medical research

Open Access Full Text Article

ORIGINAL RESEARCH

pH-triggered charge-reversal and redox-sensitive drug-release polymer micelles codeliver doxorubicin and triptolide for prostate tumor therapy

This article was published in the following Dove Press journal:
International Journal of Nanomedicine

Chen Xu[1,*]
Ri-jin Song[2,*]
Pei Lu[2,*]
Jian-chun Chen[1]
Yong-qiang Zhou[1]
Gang Shen[1]
Min-jun Jiang[1]
Wei Zhang[2]

[1]Department of Urology, The First People's Hospital of Wujiang City, Suzhou, China; [2]Department of Urology, The First Affiliated Hospital of Nanjing Medical University, Nanjing, China

*These authors contributed equally to this work

Aim: To significantly promote cancer cell uptake and to achieve combination therapy and on-demand drug release, a pH-triggered charge-switchable and redox-responsive drug-release nanovehicle was developed in this study.

Materials and methods: The nanocarrier was constructed by conjugating 3,3′-dithiodipropionic acid-modified doxorubicin (DTPA-DOX) and 2,3-dimethylmaleic anhydride (DMA) to the side amino groups of poly(ethylene glycol)-*b*-poly(L-lysine) (PEG-*b*-PLL) and by encapsulating triptolide (TRI) into the hydrophobic core. The surface charge of the obtained nanocarriers (DA-ss-DT) can change from negative to positive in response to tumor extracellular acidity pH, and the nanocarriers capably release two drugs in response to intracellular high glutathione (GSH) environment.

Results: Compared to the control group, the in vitro cellular uptake of DA-ss-DT by human prostate cancer PC-3 cells was significantly promoted in slightly acidic conditions, and the drug could be rapidly released in the high concentration of GSH conditions. The in vitro and in vivo antitumor experiments exhibited that the DA-ss-DT nanoparticles have a great antitumor effect in comparison to the control group.

Conclusion: These findings demonstrated that the DA-ss-DT nanoparticles supply a useful strategy for promoting cellular uptake and synergetic anticancer therapy.

Keywords: combination therapy, charge reversal, redox-responsive, pH-responsive

Introduction

Prostate cancer (PCa) is one of the most common types of cancer in the USA, accounting for nearly 21% of newly diagnosed cancers and 8% of cancer-related deaths among men in 2016,[1] and it is also one of the leading causes of cancer-related deaths in males worldwide.[2] The standard first-line therapy for treating PCa is androgen deprivation therapy. However, the resistance develops in most cases, and these patients progress to more aggressive metastatic castration-resistant PCa (mCRPC).[3] The treatment of mCRPC by the chemotherapeutic drugs (such as doxorubicin [DOX], docetaxel, and enzalutamide)[4] has been shown to improve the patient's quality of life and lengthen the period of survival to a certain extent,[1] but the undesired serious side effects and the development of drug resistance have hampered its further application.[3] Therefore, there is a critical need for alternative strategies for more effective treatment of advanced PCa.

Combination drug therapy is an effective strategy used clinically to enhance the therapeutic efficacy of chemotherapy.[5,6] In comparison to single chemotherapy,

Correspondence: Wei Zhang
Department of Urology, The First Affiliated Hospital of Nanjing Medical University, No. 300, Guangzhou Road, Nanjing 210029, China
Email zhangweisir@126.com

Min-jun Jiang
Department of Urology, The First People's Hospital of Wujiang City, No.169, Park Road, Songling Town, Wujiang City, Jiangsu Province, China
Email 463161688@qq.com

submit your manuscript | www.dovepress.com
Dovepress
http://dx.doi.org/10.2147/IJN.S182197

combination regimens can sensitize cancer responsive to drugs, modulate different signaling pathways in cancer cells, and lower each drug dose to reduce side effects.[7] Moreover, combination therapy has been confirmed to overcome multidrug resistance.[8,9] DOX, a type of anthracycline antibiotic drug, has been widely used in the clinical chemotherapeutic treatment of a diverse range of malignant cancers such as prostate, lung, and breast cancers.[1] However, the serious side effects (such as hematopoietic depression, alopecia, cardiotoxicity, and gastrointestinal disorders), short half-life, and circulation time have limited the further application of DOX in the clinic.[1,10,11] Triptolide (TRI), a diterpenoid triepoxide, isolated from the plant *Tripterygium wilfordii*, is a natural product that has already been found to be highly effective against many tumors such as hepatocellular carcinoma, gastric cancer, and PCa.[12] Although TRI was initially considered by a promising chemotherapeutic agent, its potential clinical application has been limited due to its extremely high toxicity and poor solubility.[13] It is reported that the combination of TRI with other anticancer drugs resulted in synergistic effects and promoted apoptosis but did not increase the side effects.[14] Moreover, Wu et al[15] developed a reduction-sensitive drug delivery system used for codelivery of DOX and TRI, and they found that the DOX and TRI had achieved the highest synergistic therapeutic effect at the ratio of 1:0.2 (DOX/TRI). They also found that the TRI could enhance the uptake of DOX by human oral cancer KB cells.[15]

Recently, since the nanoparticles can increase the solubility of soluble drugs, prolong circulation time in the blood, enrich the drug at tumor tissue through the enhanced permeability and retention (EPR) effect, and release drug on-demand, they have been widely used in drug delivery.[16–18] Moreover, the tumor microenvironment stimuli-responsive drug delivery systems have attracted great attention in cancer therapy. It is well known that the pH value varies in normal tissues and tumor tissues; the pH value in the blood and normal tissues is about pH 7.4, but the pH value in tumor tissues is slightly acidic (pH=6.5–7.2 in tumor tissues; pH=4.5–6.5 in endosomes and lysosomes).[19–21] In addition, the concentration of glutathione (GSH) is different between the extracellular (~2.0–20 μM) and intracellular (~10 mM) environments.[22–24] Moreover, the concentration of GSH in many tumors has been reported to be fourfold higher than that of normal tissues.[18,25] Therefore, the pH- and redox-responsive drug delivery system has been widely used in cancer therapy.[21,26] For example, Wei et al[27] developed a pH- and redox-responsive nanocarrier for the codelivery of DOX and 10-hydroxycamptothecin, and such a nanodrug delivery system could effectively overcome the multi-drug resistance.

To prolong the blood circulation time of nanoparticles, nanoparticles are usually modified with polyethylene glycol (PEG). However, the PEGylation appears to hinder the cellular internalization of the nanoparticles and therefore becomes an obstacle in the full realization of therapeutic effects.[28] It is reported that the positive charge could enhance the cellular uptake of nanoparticles.[21,29] Therefore, many surface charge-switchable nanoparticles have been developed for drug delivery.[30–32] These nanoparticles could maintain negative surface charge under blood circulation, while quickly changing to positive charge at the slightly acidic tumor tissues. For example, Yuan et al[33] reported a charge-reversal nanoparticle based on zwitterionic polymers, and this nanoparticle could effectively enhance cellular uptake.

Keeping these troubles in mind, here, we developed a pH-responsive charge-reversal and redox-sensitive drug-released delivery system for the codelivery of DOX and TRI (Scheme 1). In this nanosystem, the redox-sensitive DOX prodrug (3,3′-dithiodipropionic acid-modified doxorubicin [DTPA-DOX]) and 2,3-dimethylmaleic anhydride (DMA) were conjugated to the amino groups of poly(ethylene glycol)-*b*-poly(L-lysine) (PEG-*b*-PLL) to produce the pH-sensitive and redox-sensitive part: PEG-*b*-P((LL-*g*-ss-DOX)-(LL-*g*-DMA)), and then, the TRI was encapsulated into the polymer micelles formed by PEG-*b*-P((LL-*g*-ss-DOX)-(LL-*g*-DMA)) (named as DA-ss-DT). After intravenous administration to mice, DA-ss-DT nanoparticles could ideally maintain negative surface charge in blood circulation, while quickly changing to positive when it reaches the tumor tissue, and then, DA-ss-DT could be quickly ingested by cancer cells. Finally, under high concentration of GSH intracellular, the disulfide bonds between DOX and PEG-*b*-PLL were broken, and then the nanoparticles were disassembled, and DOX and TRI were rapidly released, thereby achieving combined therapy.

Materials and methods

Materials

DOX·HCl was purchased from Beijing Huafeng United Technology Co., Ltd. (Beijing, China). TRI was obtained from Bide Pharmatech Ltd. (Shanghai, China). Amino-terminated methoxyl poly(ethylene glycol) (mPEG-NH_2; molecular weight [Mw], 5,000 Da) was purchased from JenKem Technology Co., Ltd (Beijing, China). 3,3-dithiodipropionic acid (DTPA), octanedioic acid (ODA), DMA, succinic anhydride (SA), and GSH were purchased from Aladdin Reagent company (Shanghai, China). *N*ε-benzyloxycarbonyl-L-lysine-*N*-carboxyanhydride (Lys-NCA) was synthesized by the Fuchs-Farthing method according to the literature.[34]

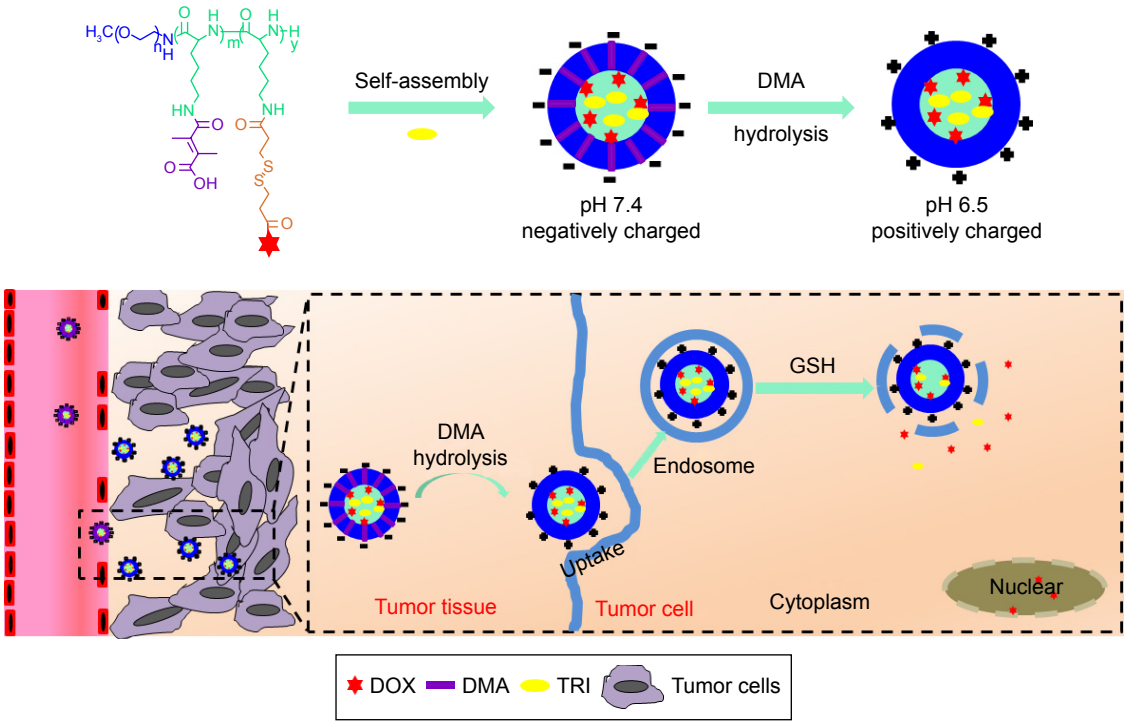

Scheme 1 Molecular structures of PEG-*b*-P((LL-*g*-ss-DOX)-(LL-*g*-DMA)) and schematic illustration of the multifunctional nanoparticles platform (DA-ss-DT) for in vivo DOX and TRI codelivery and therapy. The polymers and TRI can coassemble to form stable nanoparticles under nature conditions.

Notes: After intravenous administration to mice, the DA-ss-DT can extravasate from leaky tumor vasculature, and the surface charge of DA-ss-DT can change from negative to positive, resulting in quick cellular uptake of cancer cells. After internalization, the redox-sensitive DA-ss-DT nanoparticles disassembled quickly and released the two drugs, thus resulting in efficient tumor inhibited.

Abbreviations: DMA, 2,3-dimethylmaleic anhydride; DOX, doxorubicin; GSH, glutathione; TRI, triptolide.

MTT and Hoechst 33342 were purchased from Beyotime Institute of Biotechnology (Shanghai, China). Dry *N,N*-dimethylformamide (DMF) was purchased from Energy Chemical (Shanghai, China) and used as received.

Animal and cell line

The human PCa cell line PC-3 was obtained from Institute of Biochemistry and Cell Biology, Shanghai Institutes for Biological Sciences, Chinese Academy of Sciences (Shanghai, China) and cultured in RPMI 1640 culture medium, containing 10% (v/v) FBS, 100 IU/mL penicillin, and 100 μg/mL streptomycin at 37°C in a humidified 5% CO_2 atmosphere.

BALB/c nude mice (male; age, 4–6 weeks; weight, 20±2 g) were purchased from the Vital River Laboratory Animal Technology Co., Ltd. (Beijing, China). All animals received care in compliance with the guidelines outlined in the Guide for the Care and Use of Laboratory Animals, and all procedures were approved by the First Affiliated Hospital of Nanjing Medical University Care and Use Committee.

Synthesis of PEG-*b*-PLL block copolymer

PEG-*b*-PLL was synthesized by ring opening polymerization of Lys-NCA using mPEG-NH_2 as a macroinitiator according to the previous studies.[17,21,31] Briefly, Lys-NCA (3.93 g, 1.2 mM) was dissolved in 60 mL of dry DMF. Then, mPEG-NH_2 (2.0 g, 0.4 mM) was dissolved in 50 mL of dry DMF as the macroinitiator and added to Lys-NCA solution via a syringe under dry argon. The reaction mixture was stirred for 3 days at 40°C under a dry argon atmosphere, and then, the extra solution was evaporated to about 10 mL under reduced pressure. The resulting product was precipitated into excess ice-cold diethyl ether to obtain PEG-*b*-PLLZ.

The benzyl group of PEG-*b*-PLLZ was removed using CF_3COOH and HBr in acetic acid. In brief, PEG-*b*-PLLZ (3.0 g) was dissolved in 30 mL CF_3COOH, and then 15 mL HBr/acetic acid (33%) was added at 0°C under quick stirring and reacted for 1 hour. After that, the reaction mixture was precipitated in excessive cold diethyl ether. The product was further purified by dialyzed (molecular weight cutoff [MWCO], 3,500 Da) against distilled water. A white solid was obtained by lyophilization.

Synthesis of DTPA-DOX

DTPA-DOX was synthesized according to the previous studies.[35,36] Briefly, DTPA (100.8 mg, 0.48 mM), EDC (115.2 mg, 0.6 mM), and NHS (92 mg, 0.8 mM) were dissolved in 20 mL of dimethyl sulfoxide (DMSO), and the

reaction mixture was maintained under stirring for 1 hour at room temperature. Then, DOX·HCl (231.0 mg, 0.4 mM) and triethylamine (TEA; 0.6 mM) were dissolved in 10 mL DMSO and then added into the above-mentioned solution drop by drop under vigorous stirring, and the reaction was maintained at room temperature for 48 hours. Finally, the solution was precipitated with excessive 0.1 M diluted hydrochloric acid and washed with precold distilled water, and this step was repeated three times. The DTPA-DOX was obtained by vacuum drying.

As a control, non-redox-sensitive pro-drug ODA-DOX was synthesized through a similar procedure as mentioned earlier, just DTPA was replaced with ODA.

Synthesis of PEG-*b*-P((LL-*g*-ss-DOX)-(LL-*g*-DMA))

To obtain charge-reversal and redox-sensitive DOX-conjugated polymer, PEG-*b*-P((LL-*g*-ss-DOX)-(LL-*g*-DMA)), DTPA-DOX was conjugated to the amino groups of PEG-*b*-PLL to obtain a disulfide-contained polymer-DOX conjugate PEG-*b*-P(LL-*g*-ss-DOX) at first. In brief, DTPA-DOX (147.0 mg, 0.2 mM), EDC (57.6 mg, 0.3 mM), and NSH (46.0 mg, 0.4 mM) were dissolved in 20 mL DMSO, and the solution was maintained under stirring for 6 hours at room temperature. Then, PEG-*b*-PLL (280 mg, 0.04 mM) and a certain amount of TEA were dissolved in 30 mL DMSO and added to the above-mentioned solution drop by drop. The reaction was maintained by stirring at room temperature for 48 hours. Finally, the solution was dialyzed (MWCO, 3,500 Da) against DMSO to remove unreacted small molecules and then dialyzed against distilled water to remove DMSO, and the product PEG-*b*-P(LL-*g*-ss-DOX) was obtained by lyophilization. As a control, nonredox sensitive DOX-conjugated polymer (PEG-*b*-P(LL-*g*-cc-DOX)) was synthesized through a similar method mentioned earlier, just DTPA-DOX was replaced with ODA-DOX.

The charge-switchable and redox-sensitive conjugate polymer PEG-*b*-P((LL-*g*-ss-DOX)-(LL-*g*-DMA)) was synthesized by grafting the DMA to the extra side amino of PEG-*b*-P(LL-*g*-ss-DOX). PEG-*b*-P(LL-*g*-ss-DOX) (105.6 mg, 0.01 mM) and DMA (18.9 mg, 0.15 mM) were dissolved in 20 mL DMSO, and then, TEA (50 μL) was added under nitrogen atmosphere. The mixture solution was stirred at room temperature for 16 hours. The resulting solution was dialyzed (MWCO, 3,500 Da) against distilled at pH 8–9 for 24 hours, and the product was obtained by lyophilization.

As a control, the no-redox-sensitive but charge-switchable polymer was obtained through the reaction between DMA and PEG-*b*-P(LL-*g*-cc-DOX) by using the same method. The SA reacted with PEG-b-P(LL-*g*-ss-DOX) by using the same method mentioned above to obtain the redox-sensitive but no-charge-conversion polymer – PEG-*b*-P((LL-*g*-ss-DOX)-(LL-*g*-SA)).

DOX content in the PEG-*b*-P((LL-*g*-ss-DOX)-(LL-*g*-DA)), PEG-*b*-P((LL-*g*-cc-DOX)-(LL-*g*-DA)), and PEG-*b*-P((LL-*g*-ss-DOX)-(LL-*g*-SA)) was determined by ^{1}H nuclear magnetic resonance (NMR) and ultraviolet (UV) spectrophotometer at the wavelength of 254 nm. The DOX content was calculated according to the following formula:

$$\text{DOX\%} = \frac{\text{Weight to DOX}}{\text{Weight to polymer}} \times 100\%.$$

Preparation TRI and DOX coloaded micelle

The TRI and DOX coloaded micelles with redox-sensitive and charge reversal (named DA-ss-DT) was prepared by using the coprecipitation method. Typically, PEG-*b*-P((LL-*g*-ss-DOX)-(LL-*g*-DMA)) (15 mg) and TRI (1 mg) were dissolved in 3 mL DMSO and stirred for 1 hour at room temperature. Then, the mixture solution was added dropwise into 10 mL of ultra-purified water under vigorous stirring, then dialyzed (Mw, 3,500 Da) against water for 12 hours and filtered by a Millipore filter (pore size, 0.45 μm) to remove unencapsulated TRI. The drug loading capacity (DLC) and drug encapsulation entrapment of TRI were determined by HPLC.[13]

Moreover, the DOX and TRI coloaded micelle, which formed from PEG-*b*-P(LL-*g*-ss-DOX) (positively charged and redox-sensitive nanoparticles, abbreviated as P-ss-DT), PEG-*b*-P((LL-*g*-ss-DOX)-(LL-*g*-DMA)) (redox-insensitive but charge-switchable nanoparticles, abbreviated as DA-cc-DT), and PEG-*b*-P((LL-*g*-ss-DOX)-(LL-*g*-SA)) (no charged reversal but redox-sensitive nanoparticles [SA-ss-DT]) were prepared as the same method as DA-ss-DT, just change the PEG-*b*-P((LL-*g*-ss-DOX)-(LL-*g*-DMA)) to the corresponding polymer.

Characterization

NMR spectra were recorded on a Bruker AVANCE III spectrometer at 300 MHz with deuterated DMSO (DMSO-*d6*) or D_2O as the solvent. The size, size distribution, and the zeta potential of particles in aqueous solution were determined by dynamic light scattering (DLS; Zs90; Malvern Instruments, Malvern, UK). The morphology of particles was investigated using transmission electronic microscopy (TEM; Hitachi Ltd, Tokyo, Japan).

To study the surface charge characteristics of the particles, DA-ss-DT (0.1 mg/mL), P-ss-DT, and SA-ss-DT (0.1 mg/mL) were dispersed in PBS (pH 6.5 or 7.4, 0.1 mM) and incubated at 37°C. Samples were taken at designated time intervals, and the zeta potential was determined by DLS.

GSH-triggered micelles disassembly and drug release

The size distribution of DA-ss-DT and DA-cc-DT in response to GSH was determined by DLS measurement. In brief, 2 mL of DA-ss-DT micellar solution containing GSH (0 and 10 μM and 10 mM) was added to a glass cell placed in an incubation shaker at 37°C and stirred at 100 rpm for 8 or 24 hours. As a comparison, redox-no-sensitive DA-cc-DT micelles incubated with and without 10 mM GSH were included as controls.

The release profiles of DOX and TRI from DA-ss-DT and DA-cc-DT micelles were measured at various concentrations of GSH using a dialysis method. Typically, 3 mL of DA-ss-DT micelles containing 1.0 mg DOX was sealed in a dialysis bag (Mw, 5,000 Da) and immersed in 50 mL of PBS (pH 7.4) containing 10 μM or 10 mM GSH. Every sample was gently shaken at an appropriate speed at 37°C. At predetermined time points, 1 mL of solute outside the dialysis bag was removed and replaced with equal volume of fresh medium. The amount of the released DOX and TRI was measured using the HPLC method according to the previous study.[37]

Protein adsorption of the micelles

BSA was used as a model of plasma protein to study the protein adsorption of the micelles. The DA-ss-DT, DA-cc-DT, P-ss-DT, and SA-ss-DT micelles were separately incubated with BSA solution in PBS at pH 6.5 or 7.4, with the final concentration of micelles and proteins at 0.3 and 0.5 mg/mL, respectively. After incubation at 37°C for 2 hours, the aliquots of the samples were centrifuged at 12,000 rpm for 10 minutes. The supernatant was collected to measure the BSA concentration using the commercial BCA Protein Assay Kits.

Cellular uptake at different pHs

PC-3 cells were seeded in six-well plates at a density of 2×10^5 cells per well and incubated for 24 hours under normal culture conditions. Then, the culture medium was replaced with RPMI 1640 medium containing DA-ss-TD, P-ss-TD, and SA-ss-TD micelles at the concentration of 5 μg/mL of DOX at pH 7.4 or 6.5. After 4 hours of incubation, the cells were washed with PBS and fixed with 4% paraformaldehyde solution for 10 minutes at room temperature. The cell nuclei were stained with Hoechst 33342 for 10 minutes and then observed under an inverted fluorescence microscope (Imager A1, Zeiss, Germany).

The cellular uptake at different pHs was also measured by flow cytometry. In brief, PC-3 cells were seeded into the six-well plate at a density of 2×10^5 cells per well and incubated for 24 hours under normal culture conditions. Then, the culture medium was replaced with RPMI 1640 medium containing DA-ss-TD, P-ss-TD, and SA-ss-TD micelles at the concentration of 5 μg/mL of DOX at pH 7.4 or 6.5. After incubation for 4 hours at 37°C, the medium was removed and the cells were washed thrice with PBS. Then, 0.5 mL of trypsin was added to each well to digest the cells, and then the harvested cells were resuspended in 400 μL fresh medium for flow cytometry assay. The mean fluorescence intensity of DOX in cells was analyzed in the FL2 channel by flow cytometry (MACSQuant Analyzer 10; Miltenyi Biotec, Bergisch Gladbach, Germany).

In vitro cytotoxicity assay

First, the cytotoxicity of free drug combinations was studied by using the MTT assay. PC-3 cells were seeded in 96-well plates at a density of 5×10^3 cells per well and incubated for 24 hours. The cells were treated with free DOX+TRI (the mass ratio of DOX to TRI was 1/0, 0.9/0.1, 0.8/0.2, 0.7/0.3, 0.6/0.4, 0.5/0.5, 0.4/0.6, 0.3/0.7, 0.2/0.8, 0.1/0.9, and 0/1) for 48 hours, and the final concentration of drug was uniform at 1 μg/mL. Subsequently, MTT stock solution (20 μL, 5 mg/mL in PBS) was added to each well, and cells were further incubated for 4 hours at 37°C. Finally, cells were dissolved in 200 μL of DMSO, and the absorbance was detected at 490 nm using a microplate reader (Thermo Multiskan MK3; Thermo Fisher Scientific, Waltham, MA, USA).

Then, the cytotoxicity of PEG-*b*-PLL was also evaluated by the same MTT method.

To investigate the pH-triggered charge reversal efference, DA-ss-DT, P-ss-DT, and SA-ss-DT were evaluated against PC-3 cells at pH 7.4 or 6.5 by the MTT assay. The cells were seeded in a 96-well plate at the density of 5×10^3 cells per well. After incubation for 24 hours, the cells were treated with DA-ss-DT, P-ss-DT, or SA-ss-DT at pH 7.4 or 6.5. After 4 hours of incubation, the medium was removed, and the cells were washed twice with PBS and added to 200 μL fresh medium at pH 7.4 and incubated for 44 hours. Then, the cell viability was analyzed using the MTT method.

To investigate the sensitiveness of DA-ss-DT to reduction environment, we pretreated PC-3 cells with or without 10 mM GSH for 2 hours at 37°C. Then, the cells were washed with PBS to remove the GSH and incubated with DA-ss-DT or

DA-cc-DT containing DOX and TRI at different concentrations (mass ratio of DOX to TRI was fixed at 4:1) for further 48 hours, followed by above-mentioned steps.

In vivo antitumor efficacy

Six-week-old male BALB/c nude mice were subcutaneously injected with 4×10^6 PC-3 cells at the right flank region.[38] When the tumor size reached around 100 mm^3, the mice were randomly divided into seven groups (n=10) and intravenously injected with saline, free DOX, TRI, DOX+TRI, DA-ss-DT, DA-cc-DT, or SA-ss-DT every 3 days for three times. The tumor volume and mouse body weight were monitored every 3 days for up to 21 days after the first administration, and tumor size was calculated using the formula: Volume=0.5×(length)×(width).[2]

At the end of the experiment on antitumor efficacy, at day 21, PC-3 tumor-bearing nude mice were sacrificed, and tumor tissues were collected, fixed in 10% formalin, and embedded in paraffin blocks after dehydrating with gradient ethanol. Then, the tissues were cut into a slice and stained using H&E for histopathological evaluation.

Biodistribution

Free DOX, DA-ss-DT, and SA-ss-DT nanoparticles were administrated intravenously into nude mice bearing PC-3 tumors at an equivalent dose of 10 mg DOX per kg of mouse body weight. After 24 hours, the major organs and tissues including heart, liver, spleen, lung, kidney, and tumor were excised, washed, dried over filter paper, weighted, cut into small pieces, and homogenized. Finally, the mixture solution was extracted with chloroform/isopropanol (4:1, v/v) and centrifuged (10,000 rpm for 10 minutes); subsequently, the organic phase was collected, purified, and then analyzed by HPLC.

Statistical analyses

All the results were expressed as the mean±SD. The differences among groups were calculated using Student's *t*-test or one-way ANOVA. Differences were considered significant when $P<0.05$, $P<0.01$, and $P<0.001$.

Results and discussions

Characterization of PEG-*b*-P((LL-*g*-ss-DOX)-(LL-*g*-DMA))

The detailed synthesis route of PEG-*b*-P((LL-*g*-ss-DOX)-(LL-*g*-DMA)) was shown in Scheme S1. First, PEG-*b*-PLL and DTPA-DOX (or DOA-DOX) were synthesized; then, DTPA-DOX was grafted to the side chain of PEG-*b*-PLL through amide reaction; finally, DMA or SA was conjugated to PEG-*b*-P(LL-*g*-ss-DOX) through amide reaction.

^{1}H NMR spectra demonstrated that DTPA was successfully conjugated to DOX, and the signals at δ 2.8 ppm and 8.1 ppm were contributed to the methylene peaks of DTPA and the anthracene protons of DOX, respectively (Figure S1).[21,39]

In the spectrum of PEG-*b*-PLL and PEG-*b*-PLLZ (Figure S2), all the peaks were consistent with the previous studies.[17,21] The degree of polymerization (DP) of lysine (Z) was calculated by comparing the signal intensities of lysine methylene protons with methylene protons of PEG, and the value was 18.[17] After deprotection, the typical peaks of carbobenzoxy groups at δ 5.0 ppm and 7.1–7.4 ppm disappeared in PEG-*b*-PLL, which indicated that the deprotection was complete, and the DP of lysine in PEG-*b*-PLL was also calculated using the same method as for PEG-*b*-PLLZ, and the value also was 18.

Then, DTPA-DOX was conjugated to the side chain of PEG-*b*-PLL through amide reaction to obtain a disulfide containing polymer PEG-*b*-P(LL-*g*-ss-DOX). As shown in Figure 1, comparing the ^{1}H NMR spectrum of PEG-*b*-P(LL-*g*-ss-DOX) with DTPA-DOX, the typical signals of phenyl proton (7.0–8.0 ppm) of DOX appear, demonstrating that DTPA-DOX was successfully conjugated to PEG-*b*-PLL.

Finally, PEG-*b*-P(LL-*g*-ss-DOX) was reacted with DMA to obtain the charge-switchable polymer PEG-*b*-P((LL-*g*-ss-DOX)-(LL-*g*-DMA)). The typical peaks of DMA at δ 1.6–1.9 ppm appeared in the ^{1}H NMR spectrum of PEG-*b*-P((LL-*g*-ss-DOX)-(LL-*g*-DMA)), indicating that DMA was successfully conjugated (Figure 1). The degree of substitution of DMA on PLL is 72% by calculating through the peak area of MDA and PEG. The DOX content in PEG-*b*-P((LL-*g*-ss-DOX)-(LL-*g*-DMA)) was calculated as 11.8% (weight ratio) by comparing the peak integration of the phenyl proton of DOX with that of the PEG methylene proton signal,[17,21] and the content of DOX was measured as 9.5% by the UV spectrophotometer.[39] Because of the relative accuracy of UV spectrophotometer, we finally chose 9.5% as the content of DOX.

Synergistic cytotoxicity of DOX and TRI against PC-3 cells

To measure the optimal combination ratio of DOX and TRI, the in vitro toxicity of PC-3 cells treated with free DOX, free TRI, and free drug combination at various mass ratio (the final

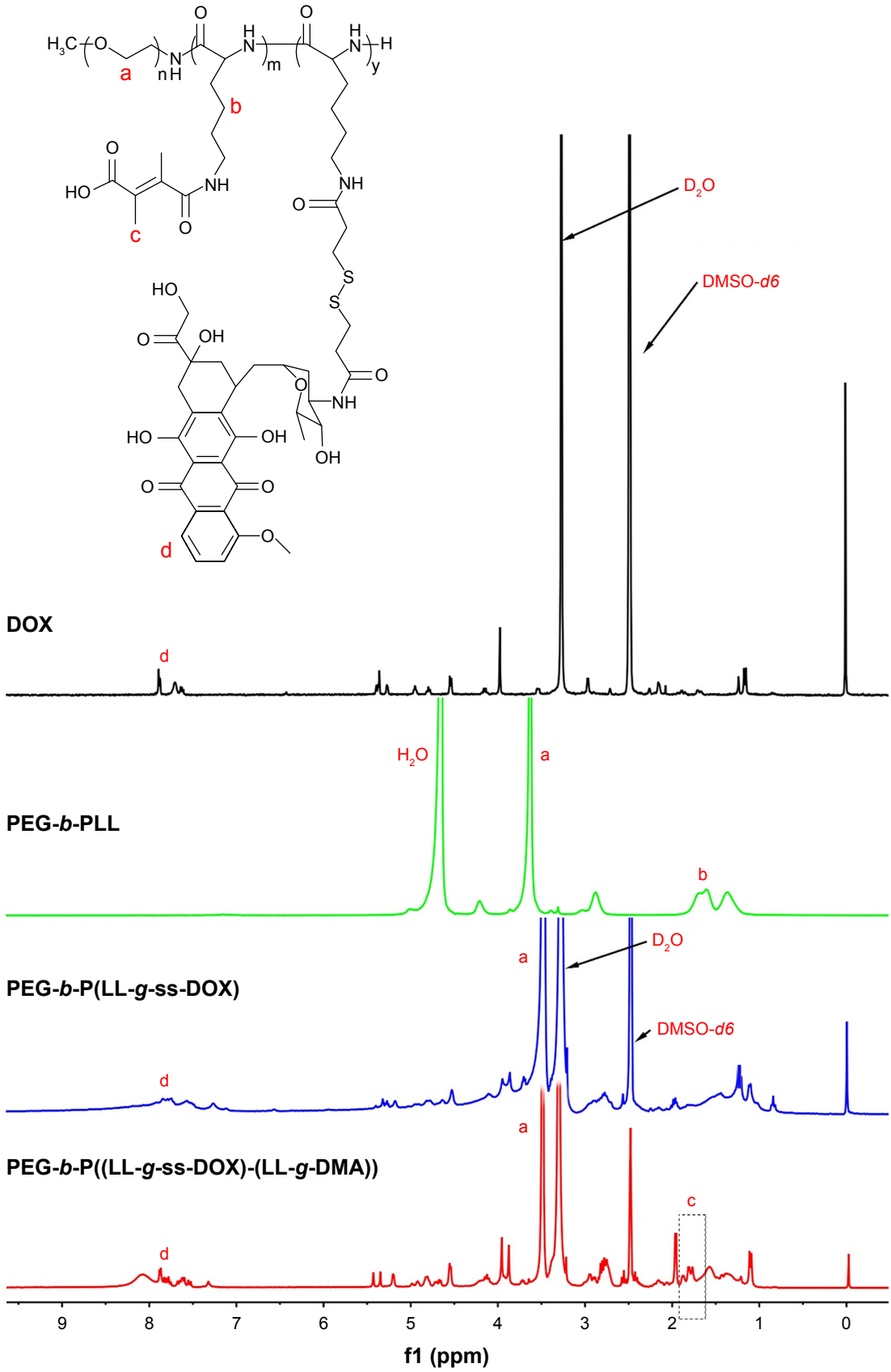

Figure 1 ^{1}H NMR spectra of DOX (in DMSO-*d6*), PEG-*b*-PLL (in D_2O), PEG-*b*-P(LL-*g*-ss-DOX) (in DMSO-*d6*), and PEG-*b*-P(LL-*g*-ss-DOX)-(LL-*g*-DMA) (in DMSO-*d6*).
Abbreviations: DMSO-*d6*, deuterated dimethyl sulfoxide; DOX, doxorubicin; NMR, nuclear magnetic resonance; PEG-*b*-PLL, poly(ethylene glycol)-*b*-poly(L-lysine).

Table 1 Characterization of DOX- and TRI-coloaded nanoparticles

Nanoparticles	Zeta (mV)	Size (nm)	PDI	DLC of DOX (%)	TRI	
					DEE (%)	DLC (%)
DA-ss-DT	−16.3±0.7	105±8	0.23±0.01	9.3±0.9	78.5±5.9	2.3±0.2
DA-cc-DT	−17.2±0.4	117±12	0.25±0.02	9.9±0.5	77.3±4.7	2.6±0.3
SA-ss-DT	−19.2±0.5	98±10	0.32±0.01	9.6±0.8	82.1±5.1	2.5±0.6
P-ss-DT	29.1±0.7	112±13	0.28±0.03	12.2±1.1	72.3±4.7	2.8±0.3

Abbreviations: DEE, drug encapsulation entrapment; DLC, drug loading capacity; DOX, doxorubicin; PDI, polydispersity index; TRI, triptolide.

concentration of drug was fixed at 1 μg/mL) was evaluated by MTT assay according to the previous study.[25] Stronger inhibitory effect on PC-3 cells viability was observed when the DOX/TRI mass ratio was 4:1 (Figure S3), and this phenomenon was different from the previous study,[15] which may be caused by drugs targeting different cancer cells. Therefore, this mass ratio was selected as the optimal ratio for the following studies.

Characterization of DOX and TRI coloaded micelles

To overcome the obstacle of nanoparticles of long circulation time and the efficient tumor cellular uptake and to achieve DOX and TRI combination therapy, we designed a nanodrug delivery system, which could achieve pH-triggered surface charge switch and redox-sensitive drug release. To determine the charger reversal ability and redox-responsive drug release property, charge reversal with redox-responsive micelle (named as DA-ss-DT), no charge switch and redox-sensitive micelle (named as SA-ss-DT), positive charge with redox-sensitive micelle (named as P-ss-DT), and charge reversal with redox-insensitive micelle (named as DA-cc-DT) were prepared by mixing TRI- and DOX-conjugated copolymers by a nanocoprecipitation method. The characterization data are shown in Table 1. The DLCs of DOX and TRI in DA-ss-DT were 9.3%±0.9% and 2.3%±0.2%, respectively. Moreover, as shown in Figure 2, the size of all micelles in aqueous solution at pH 7.4 was measured by DLS, and the values of DA-ss-DT, DA-cc-DT, SA-ss-DT, and P-ss-DT were 105±8, 117±12, 98±10, and 112±13 nm, respectively. Furthermore, the micelles' form was also detected by TEM, the images showed that all micelles were well dispersed with regular spherical shape (Figure 2A–D), and its size was about 100 nm, which was consistent with the DLS detection results (Table 1).

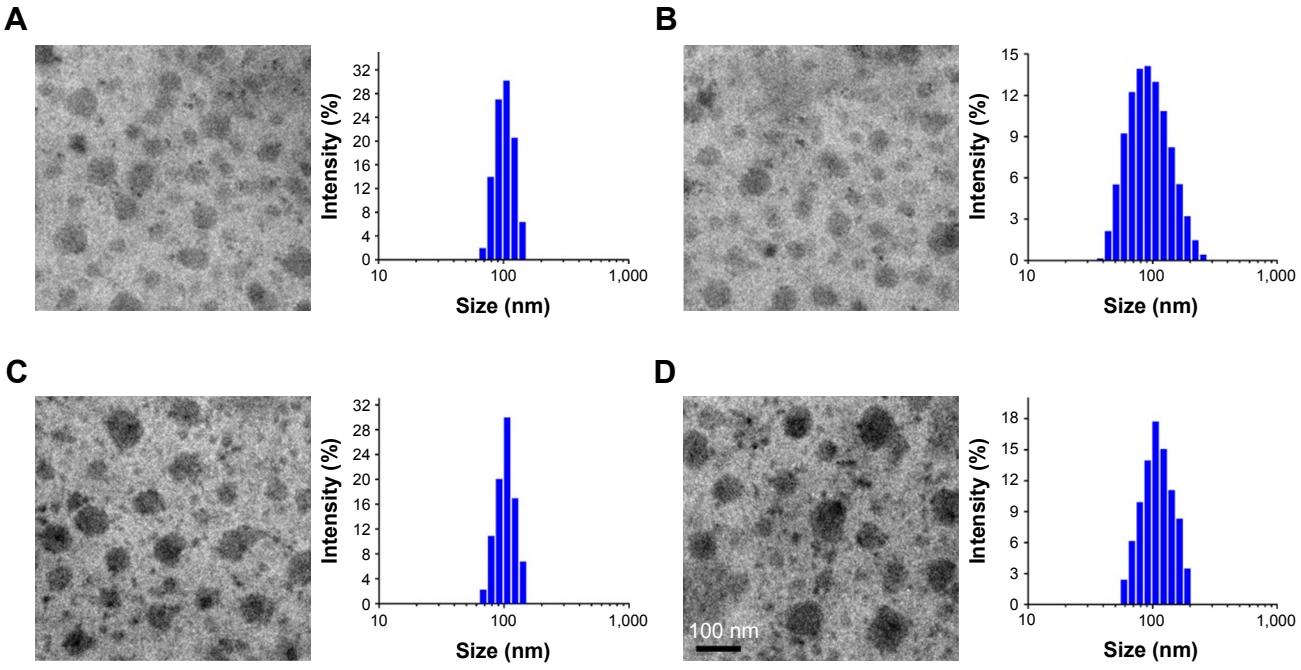

Figure 2 TEM image and size of DA-ss-DT (**A**), DA-cc-DT (**B**), SA-ss-DT (**C**), and P-ss-DT (**D**). Scale bar=100 nm.
Abbreviation: TEM, transmission electron microscopy.

Surface charge conversion behavior of DA-ss-DT

To study the pH-triggered surface charge conversion of the DA-ss-DT, the zeta potential of DA-ss-DT dispersed in the buffer solution at pH 7.4 or 6.5 was measured. As shown in Figure 3, the surface charge of P-ss-DT always maintained a positive charge at pH 7.4 or 6.5 (29.8±0.7 mV at pH 7.4 and 30±0.9 mV at pH 6.5) during the incubation time, which is ascribed to the positively charged groups (–NH_2 and –NH– in PLL). DA-ss-DT, DA-cc-DT, and SA-ss-DT at pH 7.4 had negatively charged zeta potentials of –9.5±1, –11.9±1.1, and –17±1.2 mV, respectively (Figure 3A). This can be contributed to the inertness of DMA and SA groups on the side of PLL at pH 7.4 as demonstrated by previous studies.[28,31–33,40] However, under an acidic condition, the zeta potential of DA-ss-DT and DA-cc-DT rapidly changed from negative to positive, and after incubation of 90 minutes, the zeta potentials of DA-ss-DT and DA-cc-DT were 20.3±0.8 and 19.5±0.7 mV, respectively (Figure 3B). This is ascribed to the hydrolysis of DMA-derived amides of PLL in response to the acidic environment.[40] In comparison with P-ss-DT, the surface zeta potential of DA-ss-DT and DA-cc-DT was less than P-ss-DT, which might be not all of the DMA on the side of PEG-*b*-PLL were dissociated and transformed into amino groups.[41,42] However, no significant charge-switchable behavior of SA-ss-DT was observed, and the charge of SA-ss-DT was kept at –18 mV because the SA group is more stable than DMA, and it does not easily hydrolyze under a slightly acidic environment.[43,44] These results indicated that the DA-ss-DT had a good surface charge conversion function.

Protein adsorption of DA-ss-DT

Reduced nonspecific protein adsorption of the charged nanoparticles is an important indicator for the prolonged blood circulation.[17,33] Moreover, serum protein in the blood mostly possess negative charges and readily bind onto positively charged nanoparticles through electrostatic interaction, which leads to their aggregation.[45,46] Therefore, keeping drug delivery nanoparticles negatively charged is beneficial for their stabilization in blood circulation. To demonstrate whether the surface negative charge of DA-ss-DT could reduce the nonspecific adsorption, BSA was used as a model protein to investigate the adsorption of DA-ss-DT, DA-cc-DT, SA-ss-DT, and P-ss-DT nanoparticles at pH 7.4 or 6.5. As shown in Figure S4, as a control, slightly BSA (less than 15%) was adsorbed onto SA-ss-DT nanoparticles at either pH 7.4 or 6.5 after 2 hours of incubation due to their negative charge. After 2 hours of incubation, less than 15% BSA was adsorbed onto DA-ss-DT and DA-cc-DT at pH 7.4, but ~90% BSA was adsorbed onto DA-ss-DT or DA-cc-DT nanoparticles while the pH decreased to 6.5. As a control, moreover, 90% BSA was adsorbed onto P-ss-DT at either pH 7.4 or 6.5 due to their positive charge. These BSA adsorption results further demonstrated the charge switchable property of DA-ss-DT nanoparticles at slightly acidic conditions (such as tumor tissues environments) and exhibited an additional benefit in blood circulation.

Cellular uptake of DA-ss-DT

Due to the significant role of surface charge of nanoparticles in blood circulation, protein adsorption, and cell internalization, this charge transferability was expected to endow the nanoparticles with relative selectively in cellular uptake

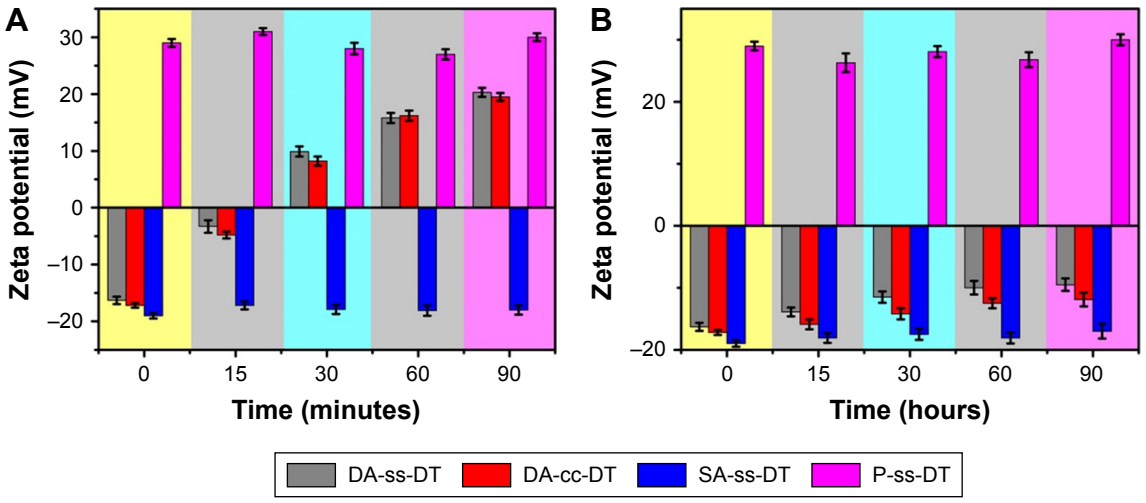

Figure 3 Zeta potential of DA-ss-DT, DA-cc-DT, SA-ss-DT, and P-ss-DT at pH 6.5 (**A**) and 7.4 (**B**) at different incubation times (mean±SD, n=3).

between normal tissues (pH, 7.2–7.4) and tumor tissues (pH, 6.2–6.9).[45] Herein, to demonstrate this hypothesis, culture medium of pH 7.4 and 6.5 were used to simulate the neutral normal tissue and slightly acidic tumor tissue extracellular environment, respectively. Huaman prostate cancer cells, PC-3 cells, were treated with DA-ss-NPs, DA-cc-NPs, SA-ss-NPs, and P-ss-NPs at pH 7.4 or 6.5 for 4 hours, and their cellular uptake was observed by fluorescence microscopy. As shown in Figure 4A, the fluorescence intensity of P-ss-NPs was the strongest in PC-3 cells at both pH 7.4 and 6.5 due to the positive charge at both pHs. However, the SA on the surface of SA-ss-DT could not hydrolyze at pH 6.5 resulting in SA-ss-DT maintaining negatively charged at pH 6.5, thus, the SA-ss-DT micelles were rarely internalized by PC-3 cells at both pH 7.4 and 6.5. Moreover, no difference was observed when the cells were incubated with DA-ss-NPs, DA-cc-NPs, and SA-ss-NP at pH 7.4. As expected, when the pH value was decreased to 6.5, the fluorescence intensity in PC-3 cells of DA-ss-DT and DA-cc-DT was remarkably stronger than that of SA-ss-DT and nearly similar to that of P-ss-DT. Thus, the nanoparticles exhibited obvious selectively in cellular uptake between different pH environments.

This different cellular uptake phenomenon induced by the charge reversal property was further demonstrated by flow cytometry analysis. The intracellular concentrations of DOX after incubation for 4 hours at different pH values were quantitatively evaluated by flow cytometry. As shown in Figure 4B and C, when cells treated with P-ss-DT at pH 7.4 or 6.5, the intracellular concentration of DOX had no significant difference and was the highest. In contrast, after treated with SA-ss-DT for a different time at pH 6.5, the intracellular concentration of DOX was the least. The intracellular concentration of DOX in PC-3 cells after treated with DA-ss-DT and DA-cc-DT was no significant in comparison with that of SA-ss-DT at pH 7.4. While the pH was decreased to 6.5, the intracellular concentration of DOX in both DA-ss-DT and DA-cc-DT groups was significantly higher than that of

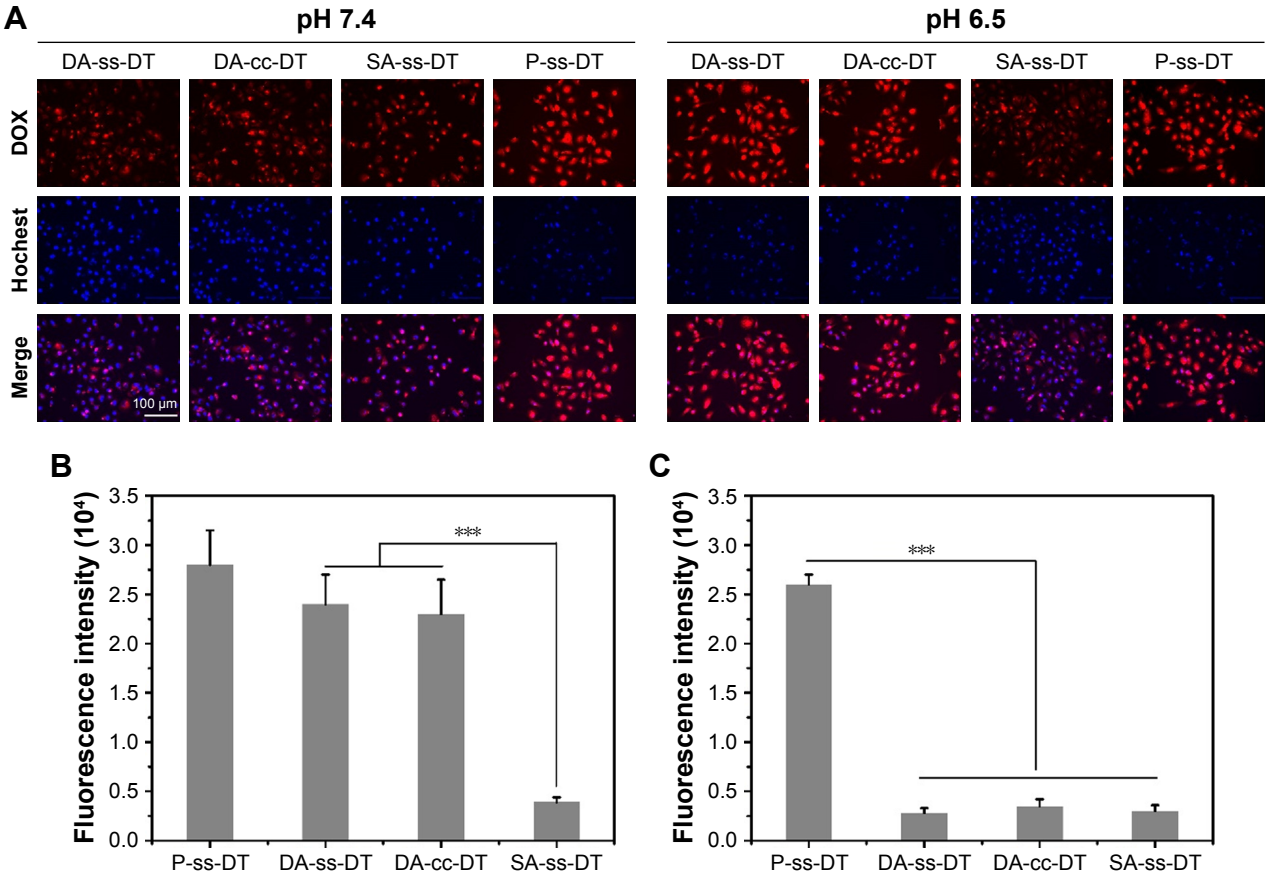

Figure 4 Cellular uptake of nanoparticles at different pHs.
Notes: (**A**) Fluorescence microscopy images of PC-3 cells incubated with DA-ss-DT, DA-cc-DT, SA-ss-DT, and P-ss-DT at pH 6.5 and 7.4 for 4 hours (scale bar=100 μm). (**B** and **C**) Fluorescence intensity of PC-3 cells treated with DA-ss-DT, DA-cc-DT, SA-ss-DT, and P-ss-DT at pH 6.5 and 7.4 for 4 hours. ***$P<0.001$. Data are represented as mean±SD (n=3).
Abbreviation: DOX, doxorubicin.

cultured with SA-ss-DT. These results were consistent with the qualitative results.

Redox-responsive micelles disassembly and drug release

The time-dependent size change of DA-ss-DT and DA-cc-DT in PBS containing different concentrations of GSH was detected by DLS to determine the reduction-triggered destabilization. As shown in Figure 5A and B, the DA-cc-DT nanoparticles were stable under different environments, even stable in 10 mM GSH after incubated for 24 hours, while the size of DA-ss-DT nanoparticles increased from 155 to 880 nm and the polydispersity index (PDI) changed from 0.21 to 0.73 (data not shown) after incubating with 10 mM GSH for 8 hours, which may contribute to the cleavage of the disulfide bond under reduction environments.[24,47] Moreover, when incubation time prolonged to 24 hours, the size of DA-ss-DT changed to 970 nm, and the PDI was 0.82. However, the DA-ss-DT could be maintained stably after incubating with 10 μM GSH for 24 hours. These results indicated that the DA-ss-DT has a good redox-sensitive ability.

Because the concentration of GSH was different in extracellular (~2.0–20 μM) and intracellular (~10 mM) environments, and it was also different between normal tissues and tumor tissues (the concentration of GSH in tumor tissues is fourfold than that in normal tissues),[48] we chose pH 7.4 buffer with 10 μM GSH or 10 mM GSH to simulate the microenvironment of plasma and tumor, respectively.[36,47] As shown in Figure 5C, little DOX release was observed in DA-cc-DT micelles within 48 hours in the presence of 10 mM GSH. In DA-ss-DT micelles, little DOX was released under 10 μM GSH; the reason may be that under this condition, the GSH content was too low to cleave the disulfide bond in DA-ss-DT.[36] When the concentration of GSH increased to 10 mM, the release of DOX from DA-ss-DT nanoparticles

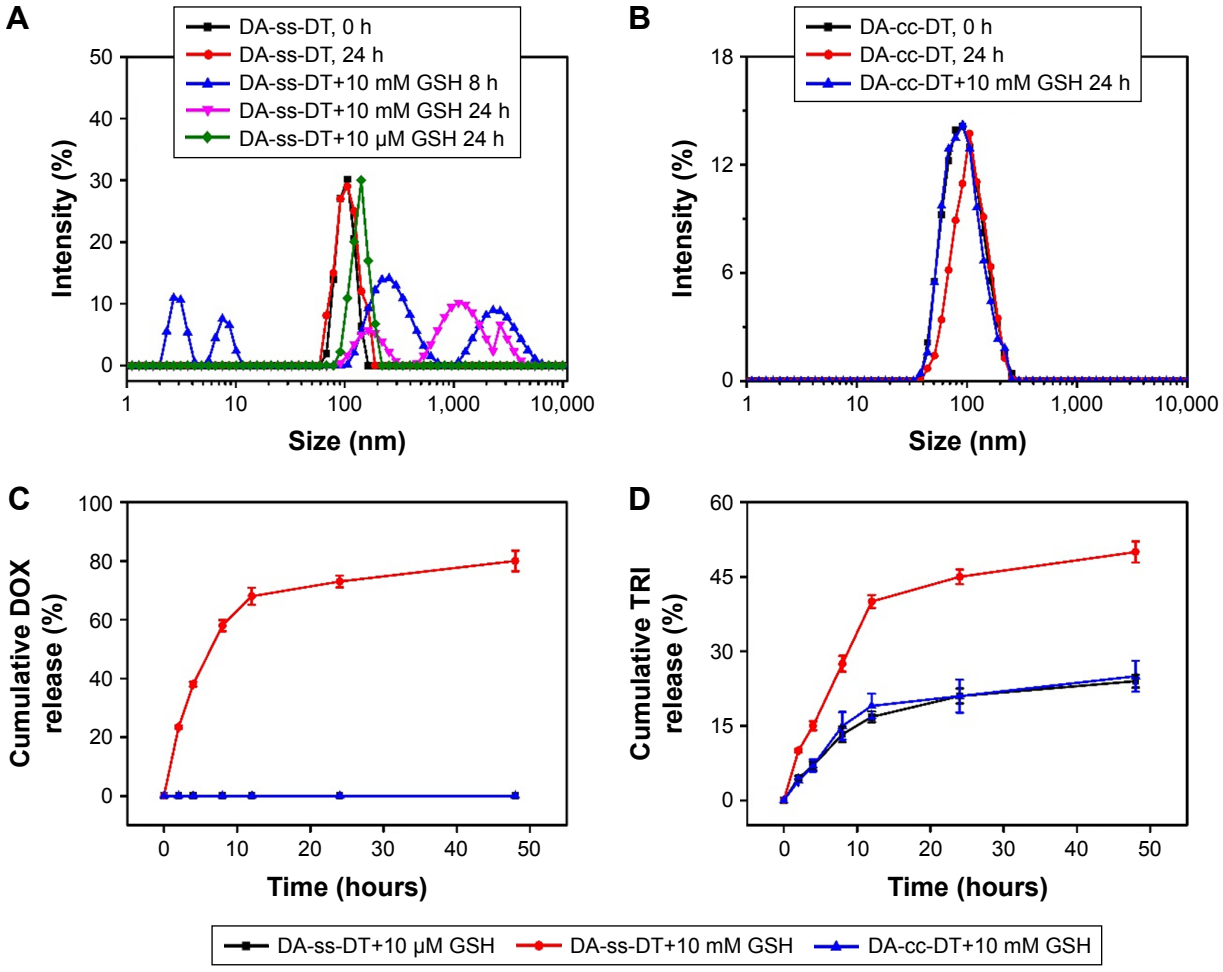

Figure 5 Size distribution of DA-ss-DT (**A**) and DA-cc-DT (**B**) in response to GSH determined by DLS measurement. Reduction-triggered release of DOX (**C**) and TRI (**D**) from DA-ss-DT and DA-cc-DT nanoparticles in PBS (pH 7.4) with 10 μM GSH. Data are represented as mean±SD (n=3).
Abbreviations: DOX, doxorubicin; DLS, dynamic light scattering; GSH, glutathione; TRI, triptolide.

was accelerated, about 78% of DOX was released within 48 hours. The TRI release profiles of DA-ss-DT and DA-cc-DT nanoparticles were shown in Figure 5D. DA-ss-DT showed a slow release of TRI in the presence of 10 μM GSH and only 25% of the total TRI within 48 hours. In the presence of 10 mM GSH, TRI released from DA-ss-DT nanoparticles was drastically accelerated and 50% of TRI was released after 48 hours, while no acceleration in TRI release was observed for DA-cc-DT nanoparticles. This is likely due to the disassembly of micelles induced by GSH. These results suggested that the nanodrug delivery system remains to maintain stable during blood circulation and maximize the retention of DOX and TRI without leakage. However, when they were enriched in the tumor tissues, the drug could be released quickly from the nanoparticles under the triggering of GSH to kill the tumor cells.

In vitro cytotoxicity assay

To investigate the toxicity of PEG-*b*-PLL, PC-3 cells were cocultured with PEG-*b*-PLL at concentrations ranging from 3.5 to 500 μg/mL. As shown in Figure S5, compared with the blank control, PC-3 cells were not influenced by the addition of PEG-*b*-PLL at any concentration, proving the noncytotoxicity of the PEG-*b*-PLL.

The in vitro cytotoxicity of all nanoparticles was also evaluated using the MTT assay against PC-3 cells in pH 6.5 and 7.4. As shown in Figure 6A and B, after incubation for 48 hours, there was no significant difference in cell viability of PC-3 cells after treated with positively charged P-ss-DT micelles at pH 7.4 or 6.5, and the cell viability of P-ss-DT treatment was obviously lower than that of other micelles. As control, there was no significant difference in the cell viability of PC-3 cells treated with

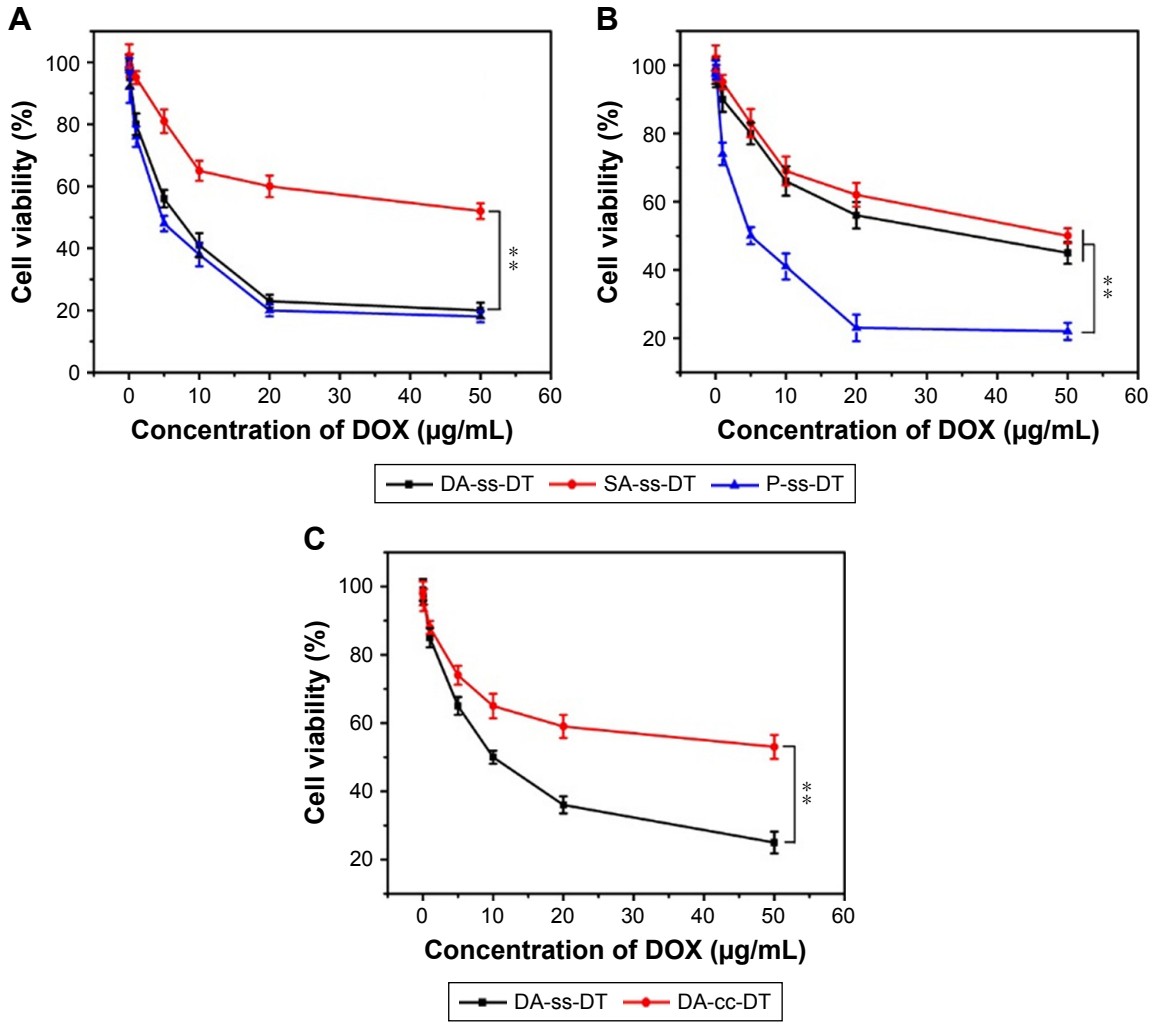

Figure 6 In vitro cytotoxicity of different drug forms to PC-3 cells under different conditions. Cell viability of PC-3 after treated with DA-ss-DT, SA-ss-DT, and P-ss-DT at pH 6.5 (**A**) and 7.4 (**B**). (**C**) Cell viability of DA-ss-DT and DA-cc-DT incubated with 1 mM GSH to PC-3 cells for 48 hours. All data are represented as mean±SD (n=6). $^{**}P<0.01$.

Abbreviations: DOX, doxorubicin; GSH, glutathione.

negatively charged SA-ss-NPs under pH 7.4 and 6.5. Moreover, the cell viability of PC-3 cells treated with charge-reversal DA-ss-DT micelles was about 50% at pH 7.4 even if the highest concentration reached 50 μg/mL. In contrast, the cell viability of PC-3 cells incubated with charge-reversal DA-ss-DT micelles could be less than 20% under pH 6.5, which is close to the cell viability of PC-3 cells treated with P-ss-DT. These results indicated that the charge-switchable DA-ss-DT more effectively inhibited the proliferation of PC-3 cells at pH 6.5 than at pH 7.4, and DA-ss-DT showed a more effective inhibition proliferation against cancer cells at tumor tissues pH 6.5 than noncharge-switchable SA-ss-DT, as described in the previous studies.[21]

Furthermore, to investigate the redox-responsive drug release in tumor cells and enhance the therapy effect, the PC-3 cells were incubated with 10 mM GSH for 2 hours at first and then replaced with fresh RPMI 1640 containing DA-ss-DT and DA-cc-DT for another 48 hours. As shown in Figure 6C, the cell viability of PC-3 cells after treated with DA-ss-DT was significantly lower than that of DA-cc-DT. Moreover, the half maximal inhibitory concentration (IC_{50}) of DA-cc-DT (75.8 μg/mL) was nine times higher than those treated with DA-ss-DT (8.5 μg/mL). This phenomenon contributed to the effect of disulfide linkages in the nanoparticles. A similar phenomenon was also observed in the previous studies.[21,49]

Enhanced tumor accumulation and reduced systemic toxicity in vivo

We assumed that the charge-reversal nanoparticles could enhance the tumor accumulation and reduce systemic toxicity, and the biodistribution was studied to validate this hypothesis. The DOX accumulated in principal organs and tissues on PC-3 orthodox PCa xenograft models for 24 hours after being injected with formulations was analyzed by HPLC. As shown in Figure S6, only a litter DOX was detected in all major organs but exhibited significant accumulation in the heart, which suggested that the injection of free DOX might lead to unavoidable cardiotoxicity and unsatisfied antitumor effects. Moreover, DA-ss-NPs showed ~1.8-fold accumulation in tumor sites in comparison with SA-ss-NPs, where only a trace amount was seen in the heart. This significant enhanced tumor accumulation of the DA-ss-DT is attributed to the change of the surface charge from negative to positive, which is triggered by the tumor extracellular acidity.[33] Furthermore, the nanoparticles exhibited significant accumulation in the liver and spleen, which might be due to the capture of reticular endothelial system.[50]

In vivo antitumor efficiency

The in vivo therapeutic efficacy of different drug forms was evaluated in a PC-3 mouse tumor model. Tumor-bearing mice were randomly divided into seven groups with eight mice in each group: PBS, free DOX, free TRI, free DOX+TRI, DA-ss-DT, DA-cc-DT, and SA-ss-DT. When the tumor grew to a size of about 50–100 mm^3, 1 week after inoculation of the cancer cells, different formulations with equivalent doses of DOX (5.0 mg/kg) and TRI (1.25 mg/kg) were injected intravenously via tail on days 0, 3, and 6. The tumor size was observed and measured every 3 days for 21 days. As shown in Figure 7A, all the drug formulations have the obvious inhibitory effect on tumor growth to the different degree compared with the PBS control group. In the free drugs group, we found that the combination therapy of DOX and TRI was more effective than the use of a single drug. Moreover, because of the EPR effect of nanoparticles, SA-ss-DT exhibited better therapeutic effect compared with the combination of free DOX and TRI. However, the DA-cc-DT showed a less antitumor effect compared with SA-ss-DT group, which may be the drugs was not effectively released. The most effective therapeutics was the DA-ss-DT-treated group, with a significant inhibition of tumor growth during the whole treatment. Furthermore, the tumor volume of DA-ss-DT-treated group was 3.2-, 6.5- and 1.8-fold smaller than that treated with free DOX+TRI, DA-cc-DT, and SA-ss-DT, respectively. The highest antitumor effect of DA-ss-DT may be contributed to the passive targeting, rapid ingestion by cancer cells, responsive drug release, and the combination of synergistic effects.

Mice body weight was also recorded every 3 days, and the results are shown in Figure 7B. It can be seen that except for the body weight of free drugs-treated group, the body weight of the nanoparticles-treated groups increased during whole treatment. Loss of body weight in mice after DOX treatment may be caused by DOX's side effects.[27,35,37] Finally, the histological changes of tumors following different treatments were analyzed by H&E staining. As shown in Figure 7C, in the saline group, the tumor cells were polykaryocytes with large irregular karyons and rich cytoplasm and more nuclear division. In drug treatment groups, the tumor tissues showed altered morphology with cell damage and shrunk nuclei. The group treated with DA-ss-DT micelles exhibited the largest necrosis area, further validating the best antitumor activity of this pH- and redox-responsive combination therapy.

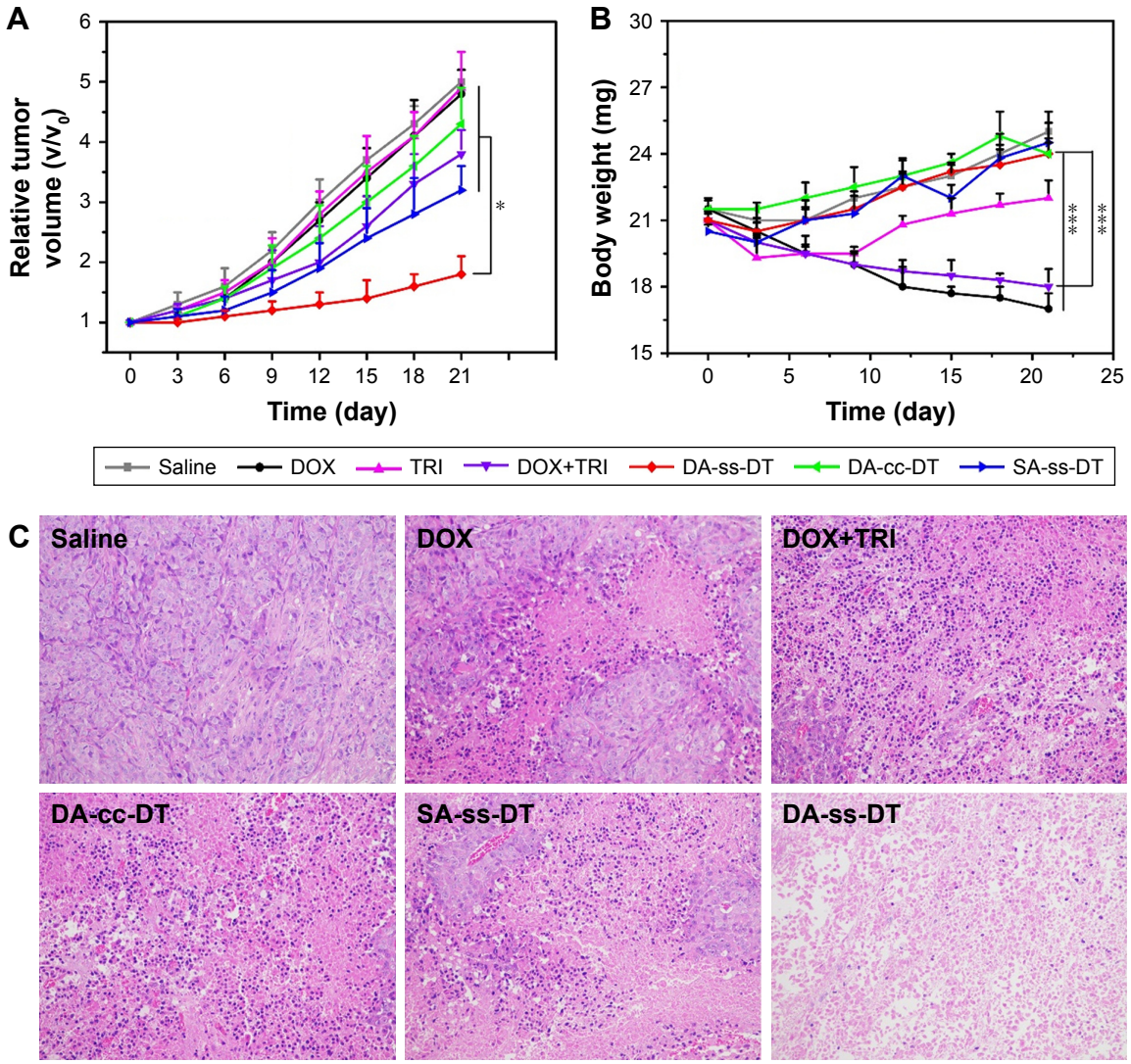

Figure 7 In vivo antitumor effects of DOX, TRI, DOX+TRI, DA-ss-DT, DA-cc-DT, and SA-ss-DT. Relative tumor volume (**A**) and body weight (**B**) of PC-3-bearing nude mice after treated with different drug forms. (**C**) Tumor tissue sections (stained by H&E) of mice from different groups. The sale bar is 50 μm for all images. *$P<0.05$ and ***$P<0.001$. Data are represented as mean±SD (n=6).
Abbreviations: DOX, doxorubicin; TRI, triptolide.

Conclusion

We have successfully designed a pH- and redox-responsive polymer drug-conjugated nanosystem for the codelivery of DOX and TRI. The charge-switchable DA-ss-DT was well synthesized through the conjugated of DTPA-DOX and DMA to the side link amino groups of PEG-b-PLL. The surface charge of DA-ss-DT could change from negative at blood pH to positive at tumor extracellular pH. The charge reversal ability could enhance the cellular uptake of nanoparticles in the tumor extracellular environment. Subsequently, after internalized by cancer cells, the disulfide bond in the nanoparticles was cleaved by intracellular redox conditions, leading to rapid drug release, which in turn resulted in increased inhibition of tumor growth. In addition, the codelivery of DOX and TRI significantly enhanced the therapeutic efficiency. Since the contradiction of nanoparticles with prolonging circulation time, efficient cellular uptake, and codelivery of two drugs are the great challenges in drug delivery in the present, the DA-ss-DT nanoparticles with pH-triggering surface charge-reversal and redox-responsive drug release overcome these three factors and hence have a great potential to achieve better therapeutic effects in cancer treatment.

Acknowledgment

This research was financially supported by the Talent Health Youth Project of Suzhou city (grant number: GGRC052).

Disclosure

The authors report no conflicts of interest in this work.

References

1. Zhao K, Li D, Xu W, et al. Targeted hydroxyethyl starch prodrug for inhibiting the growth and metastasis of prostate cancer. *Biomaterials*. 2017;116:82–94.
2. Desantis CE, Siegel RL, Sauer AG, et al. Cancer statistics for African Americans, 2016: progress and opportunities in reducing racial disparities. *CA Cancer J Clin*. 2016;66(4):290–308.
3. Xu X, Wu J, Liu Y, et al. Multifunctional envelope-type siRNA delivery nanoparticle platform for prostate cancer therapy. *ACS Nano*. 2017;11(3):2618–2627.
4. Farokhzad OC, Cheng J, Teply BA, et al. Targeted nanoparticle-aptamer bioconjugates for cancer chemotherapy in vivo. *Proc Natl Acad Sci U S A*. 2006;103(16):6315–6320.
5. Ruttala HB, Chitrapriya N, Kaliraj K, et al. Facile construction of bioreducible crosslinked polypeptide micelles for enhanced cancer combination therapy. *Acta Biomater*. 2017;63:135–149.
6. Zhang R, Ru Y, Gao Y, Li J, Mao S. Layer-by-layer nanoparticles co-loading gemcitabine and platinum (IV) prodrugs for synergistic combination therapy of lung cancer. *Drug Des Devel Ther*. 2017;11:2631–2642.
7. Hu Q, Sun W, Wang C, Gu Z. Recent advances of cocktail chemotherapy by combination drug delivery systems. *Adv Drug Deliv Rev*. 2016;98:19–34.
8. Qin SY, Cheng YJ, Lei Q, Zhang AQ, Zhang XZ. Combinational strategy for high-performance cancer chemotherapy. *Biomaterials*. 2018;171:178–197.
9. Zhao L, Wientjes MG, Au JL, Jl A. Evaluation of combination chemotherapy: integration of nonlinear regression, curve shift, isobologram, and combination index analyses. *Clin Cancer Res*. 2004;10(23):7994–8004.
10. Xu W, Ding J, Xiao C, et al. Versatile preparation of intracellular-acidity-sensitive oxime-linked polysaccharide-doxorubicin conjugate for malignancy therapeutic. *Biomaterials*. 2015;54:72–86.
11. Octavia Y, Tocchetti CG, Gabrielson KL, Janssens S, Crijns HJ, Moens AL. Doxorubicin-induced cardiomyopathy: from molecular mechanisms to therapeutic strategies. *J Mol Cell Cardiol*. 2012;52(6):1213–1225.
12. Liu Q. Triptolide and its expanding multiple pharmacological functions. *Int Immunopharmacol*. 2011;11(3):377–383.
13. Ling D, Xia H, Park W, et al. pH-sensitive nanoformulated triptolide as a targeted therapeutic strategy for hepatocellular carcinoma. *ACS Nano*. 2014;8(8):8027–8039.
14. Sai K, Li WY, Chen YS, et al. Triptolide synergistically enhances temozolomide-induced apoptosis and potentiates inhibition of NF-κB signaling in glioma initiating cells.[J]. *Am J Chin Med*. 2014;42(2):485–503.
15. Wu B, Lu ST, Zhang LJ, Zhuo RX, Xu HB, Huang SW. Codelivery of doxorubicin and triptolide with reduction-sensitive lipid-polymer hybrid nanoparticles for in vitro and in vivo synergistic cancer treatment. *Int J Nanomedicine*. 2017;12:1853–1862.
16. Tao X, Gou J, Zhang Q, et al. Synergistic breast tumor cell killing achieved by intracellular co-delivery of doxorubicin and disulfiram via core-shell-corona nanoparticles. *Biomater Sci*. 2018;6(7):1869–1881.
17. Huo Q, Zhu J, Niu Y, et al. pH-triggered surface charge-switchable polymer micelles for the co-delivery of paclitaxel/disulfiram and overcoming multidrug resistance in cancer. *Int J Nanomedicine*. 2017;12:8631–8647.
18. Zhu J, Niu Y, Li Y, et al. Stimuli-responsive delivery vehicles based on mesoporous silica nanoparticles: recent advances and challenges. *J Mater Chem B*. 2016;5.
19. Cheng X, Li D, Lin A, et al. Fabrication of multifunctional triple-responsive platform based on CuS-capped periodic mesoporous organosilica nanoparticles for chemo-photothermal therapy. *Int J Nanomedicine*. 2018;13:3661–3677.
20. Jin M, Jin G, Kang L, Chen L, Gao Z, Huang W. Smart polymeric nanoparticles with pH-responsive and PEG-detachable properties for co-delivering paclitaxel and survivin siRNA to enhance antitumor outcomes. *Int J Nanomedicine*. 2018;13:2405–2426.
21. Wang Y, Lv S, Deng M, Tang Z, Chen X. A charge-conversional intracellular-activated polymeric prodrug for tumor therapy. *Polym Chem*. 2016;7(12):2253–2263.
22. Cheetham AG, Chakroun RW, Ma W, Cui H. Self-assembling prodrugs. *Chem Soc Rev*. 2017;46(21):6638–6663.
23. Zhang J, Fang X, Li Z, et al. Redox-sensitive micelles composed of disulfide-linked Pluronic-linoleic acid for enhanced anticancer efficiency of brusatol. *Int J Nanomedicine*. 2018;13:939–956.
24. Lin J, Zhao C, Liu C, et al. Redox-responsive F127-folate/F127-disulfide bond-d-α-tocopheryl polyethylene glycol 1000 succinate/P123 mixed micelles loaded with paclitaxel for the reversal of multidrug resistance in tumors. *Int J Nanomedicine*. 2018;13:805–830.
25. Li J, Xu R, Lu X, He J, Jin S. A simple reduction-sensitive micelles co-delivery of paclitaxel and dasatinib to overcome tumor multidrug resistance. *Int J Nanomedicine*. 2017;12:8043–8056.
26. Tan S, Wang G, Redox-Responsive WG. Redox-responsive and pH-sensitive nanoparticles enhanced stability and anticancer ability of erlotinib to treat lung cancer in vivo. *Drug Des Devel Ther*. 2017;11:3519–3529.
27. Wei X, Wang Y, Xiong X, et al. Codelivery of a π-π stacked dual anticancer drug combination with nanocarriers for overcoming multidrug resistance and tumor metastasis. *Adv Funct Mater*. 2016;26(45):8266–8280.
28. Wu L, Wu M, Lin X, et al. Magnetite nanocluster and paclitaxel-loaded charge-switchable nanohybrids for MR imaging and chemotherapy. *J Mater Chem B*. 2016;5.
29. Chen S, Rong L, Lei Q, et al. A surface charge-switchable and folate modified system for co-delivery of proapoptosis peptide and p53 plasmid in cancer therapy. *Biomaterials*. 2016;77:149–163.
30. Chen WL, Li F, Tang Y, et al. Stepwise pH-responsive nanoparticles for enhanced cellular uptake and on-demand intracellular release of doxorubicin. *Int J Nanomedicine*. 2017;12:4241–4256.
31. Lim C, Sim T, Hoang NH, et al. A charge-reversible nanocarrier using PEG-PLL (-*g*-Ce6, DMA)-PLA for photodynamic therapy. *Int J Nanomedicine*. 2017;12:6185–6196.
32. Feng S, Zhang H, Zhi C, Gao XD, Nakanishi H. pH-responsive charge-reversal polymer-functionalized boron nitride nanospheres for intracellular doxorubicin delivery. *Int J Nanomedicine*. 2018;13:641–652.
33. Yuan YY, Mao CQ, du XJ, et al. Surface charge switchable nanoparticles based on zwitterionic polymer for enhanced drug delivery to tumor. *Adv Mater*. 2012;24(40):5476–5480.
34. Deng C, Chen X, Yu H, et al. A biodegradable triblock copolymer poly(ethylene glycol)-b-poly(l-lactide)-b-poly(l-lysine): Synthesis, self-assembly, and RGD peptide modification. *Polymer*. 2007;48(1):139–149.
35. Hu H, Li Y, Zhou Q, et al. Redox-sensitive hydroxyethyl starch-doxorubicin conjugate for tumor targeted drug delivery. *ACS Appl Mater Interfaces*. 2016;8(45):30833–30844.
36. Jiang Y, Wang X, Liu X, et al. Enhanced antiglioma efficacy of ultrahigh loading capacity paclitaxel prodrug conjugate self-assembled targeted nanoparticles. *ACS Appl Mater Interfaces*. 2017;9(1):211–217.
37. Wang F, Wang YC, Dou S, Xiong MH, Sun TM, Wang J. Doxorubicin-tethered responsive gold nanoparticles facilitate intracellular drug delivery for overcoming multidrug resistance in cancer cells. *ACS Nano*. 2011;5(5):3679–3692.
38. Yang Q, Wu L, Li L, Zhou Z, Huang Y. Subcellular co-delivery of two different site-oriented payloads for tumor therapy. *Nanoscale*. 2017;9(4):1547–1558.
39. Su Y, Hu Y, du Y, et al. Redox-responsive polymer-drug conjugates based on doxorubicin and chitosan oligosaccharide-g-stearic acid for cancer therapy. *Mol Pharm*. 2015;12(4):1193–1202.
40. du JZ, Mao CQ, Yuan YY, Yang XZ, Wang J. Tumor extracellular acidity-activated nanoparticles as drug delivery systems for enhanced cancer therapy. *Biotechnol Adv*. 2014;32(4):789–803.
41. Mura S, Nicolas J, Couvreur P. Stimuli-responsive nanocarriers for drug delivery. *Nat Mater*. 2013;12(11):991–1003.

42. du JZ, du XJ, Mao CQ, Wang J. Tailor-made dual pH-sensitive polymer-doxorubicin nanoparticles for efficient anticancer drug delivery. *J Am Chem Soc*. 2011;133(44):17560–17563.
43. Kamaly N, Yameen B, Wu J, Farokhzad OC. Degradable controlled-release polymers and polymeric nanoparticles: mechanisms of controlling drug release. *Chem Rev*. 2016;116(4):2602–2663.
44. Huang M, Zhao K, Wang L, et al. Dual stimuli-responsive polymer prodrugs quantitatively loaded by nanoparticles for enhanced cellular internalization and triggered drug release. *ACS Appl Mater Interfaces*. 2016;8(18):11226–11236.
45. Han SS, Li ZY, Zhu JY, et al. Dual-pH sensitive charge-reversal polypeptide micelles for tumor-triggered targeting uptake and nuclear drug delivery. *Small*. 2015;11(21):2543–2554.
46. Li S-X LL, Zhang L-J, et al. Synergetic enhancement of antitumor efficacy with charge-reversal and reduction-sensitive polymer micelles. *Polym Chem*. 2016;7:5113–5122.
47. Bao Y, Guo Y, Zhuang X, et al. D-α-tocopherol polyethylene glycol succinate-based redox-sensitive paclitaxel prodrug for overcoming multidrug resistance in cancer cells. *Mol Pharm*. 2014;11(9):3196–3209.
48. Sun J, Liu Y, Chen Y, et al. Doxorubicin delivered by a redox-responsive dasatinib-containing polymeric prodrug carrier for combination therapy. *J Control Release*. 2017;258:43–55.
49. Lv S, Tang Z, Zhang D, et al. Well-defined polymer-drug conjugate engineered with redox and pH-sensitive release mechanism for efficient delivery of paclitaxel. *J Control Release*. 2014;194:220–227.
50. Chen WL, Li F, Tang Y, et al. Stepwise pH-responsive nanoparticles for enhanced cellular uptake and on-demand intracellular release of doxorubicin. *Int J Nanomedicine*. 2017;12:4241–4256.

Supplementary materials

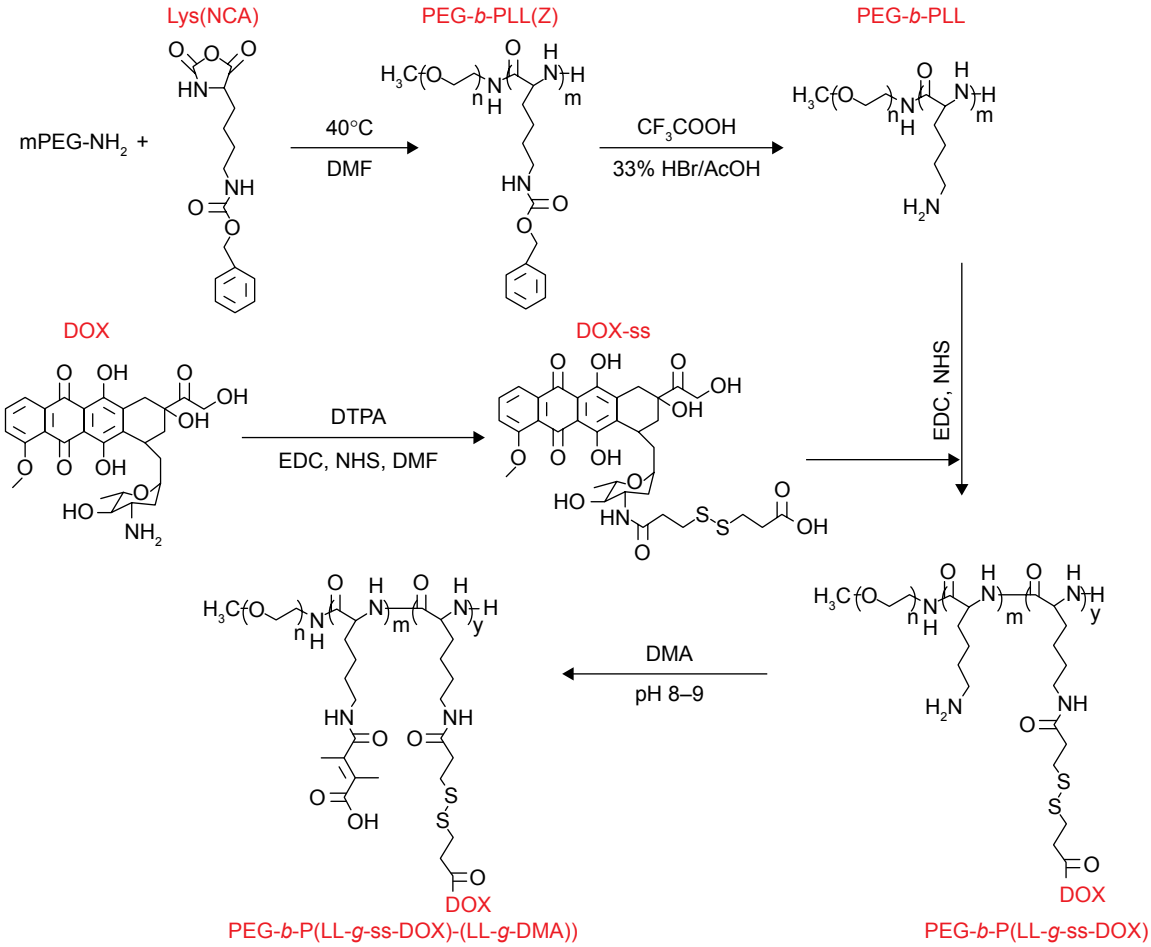

Scheme S1 The synthesis route of PEG-*b*-P((LL-*g*-ss-DOX)-(LL-*g*-DMA)).
Abbreviations: PEG-*b*-PLL, poly(ethylene glycol)-*b*-poly(L-lysine); DOX, doxorubicin; DMF, dimethylformamide; DTPA, 3,3′-dithiodipropionic acid; DMA, 2,3-dimethylmaleic anhydride; Lys(NCA), lysine-*N*-carboxyanhydride.

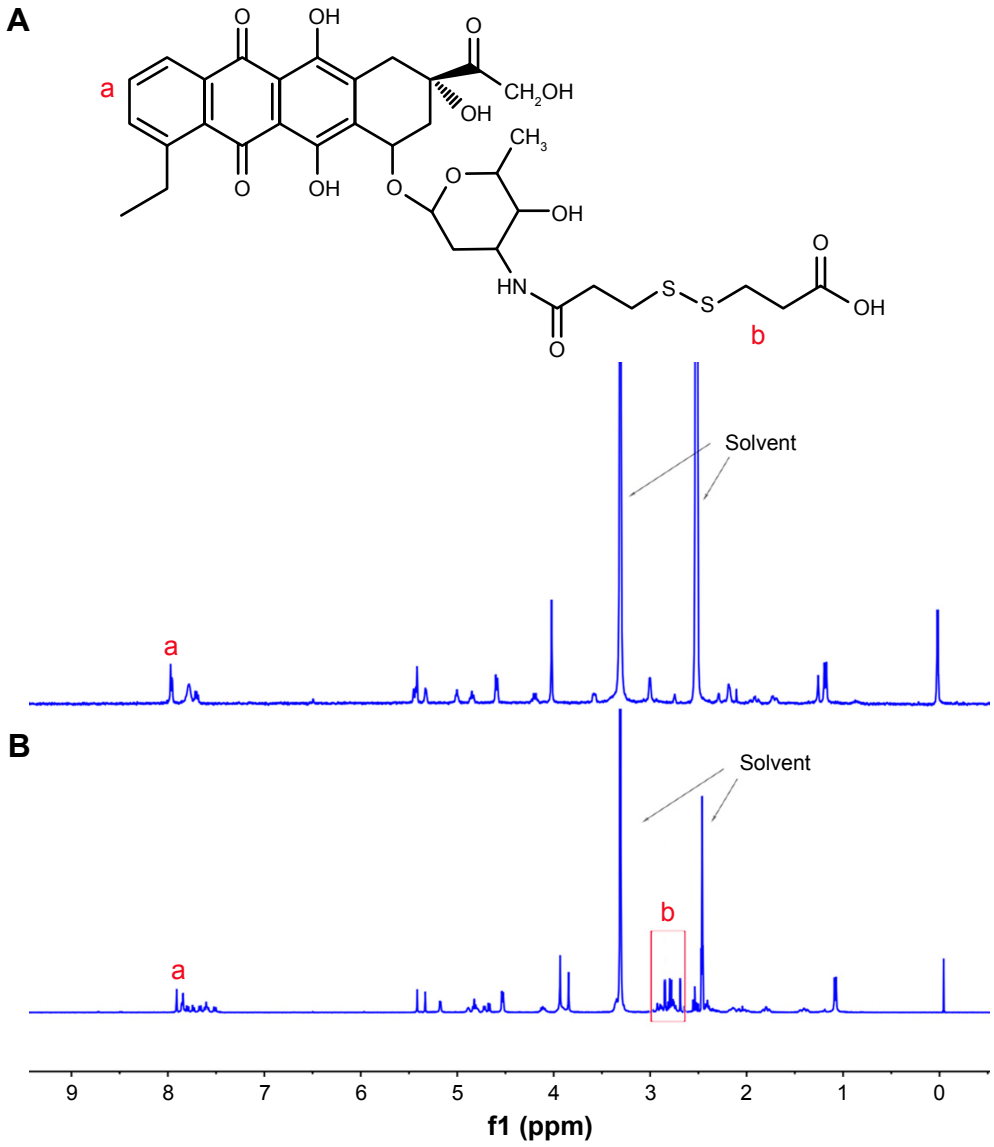

Figure S1 ^{1}H NMR spectra of DOX (**A**) and DTPA-DOX (**B**) in DMSO-*d6*.
Abbreviations: DMSO-*d6*, deuterated dimethyl sulfoxide; DOX, doxorubicin; DTPA, 3,3′-dithiodipropionic acid; NMR, nuclear magnetic resonance.

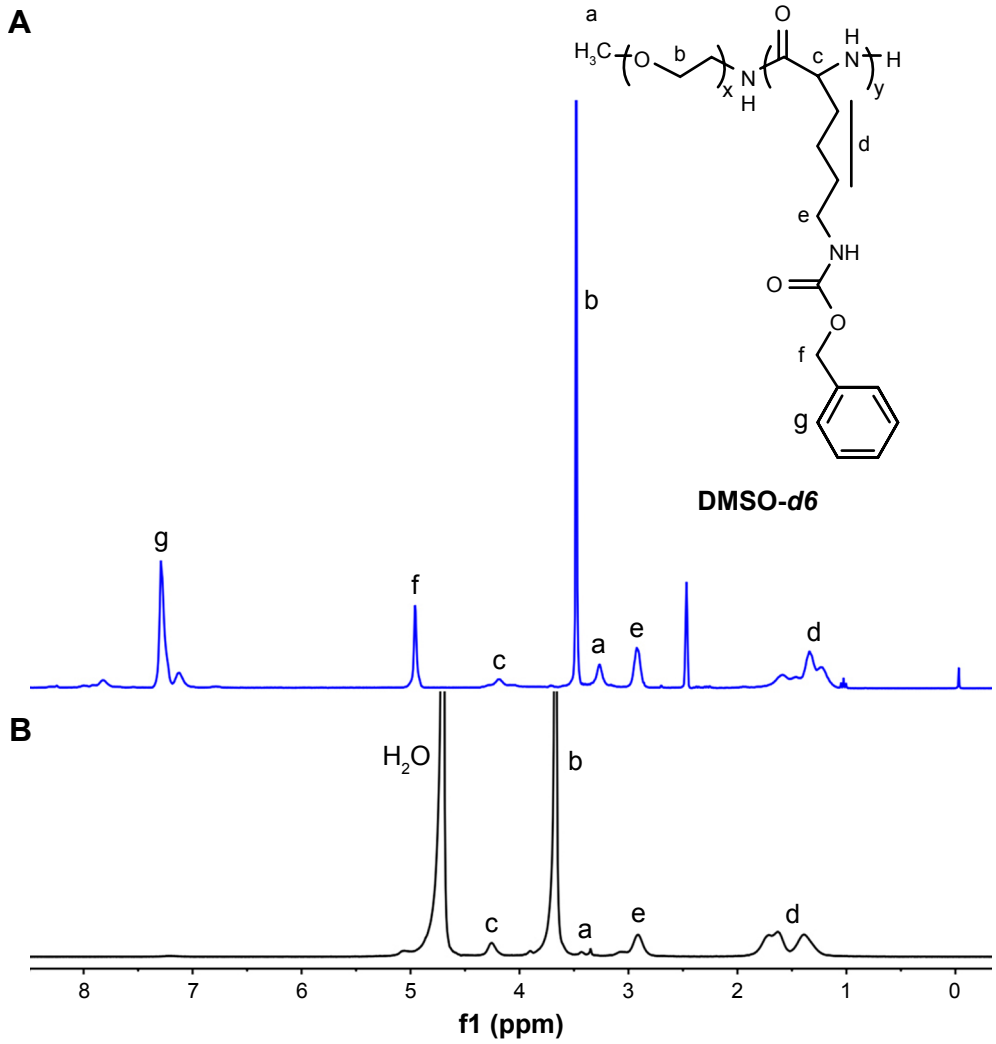

Figure S2 ^{1}H NMR spectra of PEG-*b*-PLLZ in DMSO-*d6* (**A**) and PEG-*b*-PLL (**B**) in D_2O.
Abbreviations: DMSO-*d6*, deuterated dimethyl sulfoxide; NMR, nuclear magnetic resonance; PEG-*b*-PLL, poly(ethylene glycol)-*b*-poly(L-lysine).

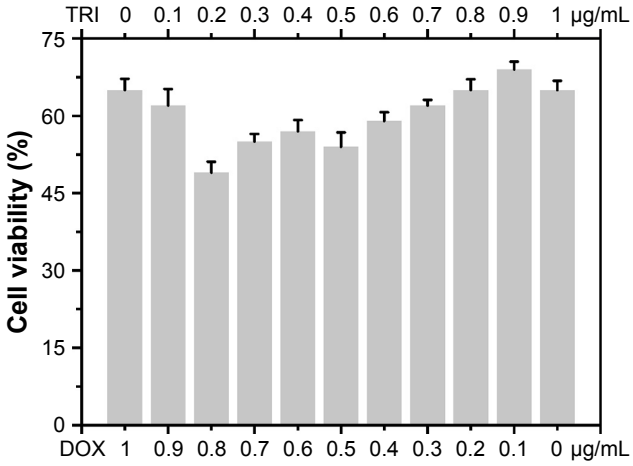

Figure S3 Viability of PC-3 cells incubated with DOX+TRI with different mass ratios of DOX to TRI for 48 hours at the drug concentration of 1 μg/mL.
Abbreviations: DOX, doxorubicin; TRI, triptolide.

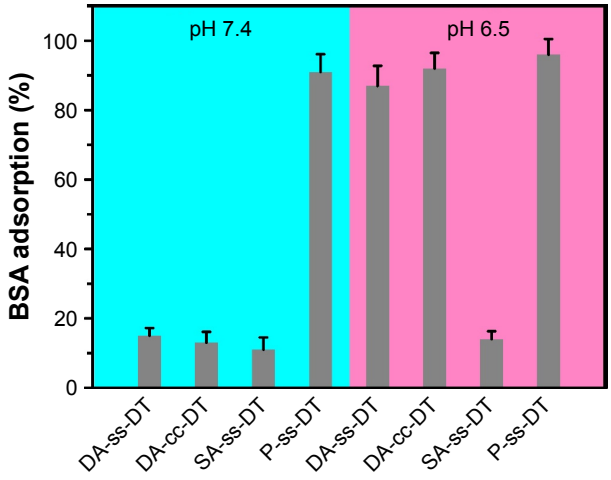

Figure S4 BSA adsorption of DA-ss-DT, DA-cc-DT, SA-ss-DT, and P-ss-DT at pH 7.4 or pH 6.5; data are represented as mean±SD (n=3).
Abbreviation: PEG-*b*-PLL, poly(ethylene glycol)-*b*-poly(L-lysine).

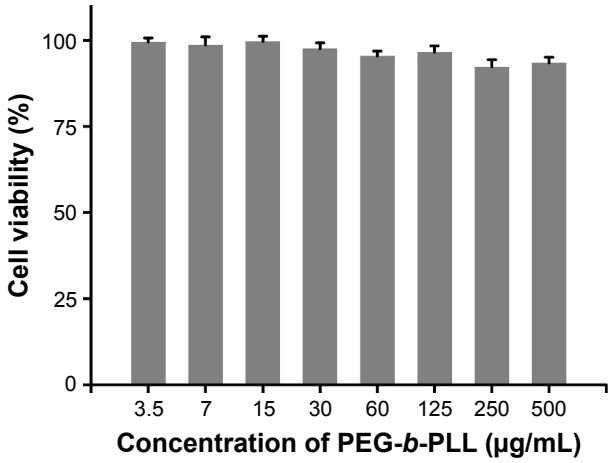

Figure S5 MTT assay of PEG-*b*-PLL in PC-3 cells after incubation for 48 h. Data showed mean±SD, n=6.
Abbreviation: PEG-*b*-PLL, poly(ethylene glycol)-*b*-poly(L-lysine).

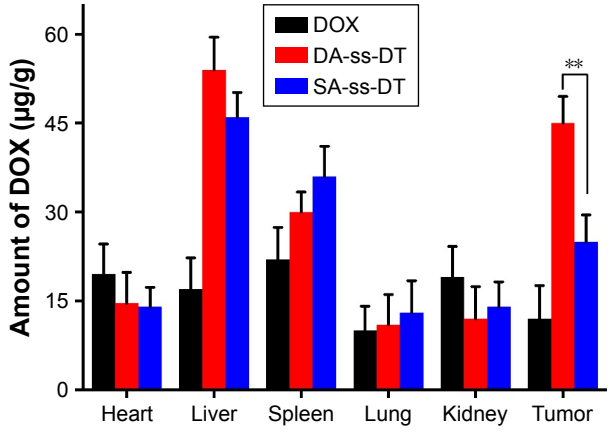

Figure S6 Tissue distribution of DOX in PC-3 tumor-bearing mice 24 h following intravenous injection of DA-ss-DT, SA-ss-DT nanoparticles or free DOX (10 mg DOX/kg). n=3, $^{**}P<0.01$.
Abbreviation: DOX, doxorubicin.